Assessing drivers of estuarine pH: A comparative analysis of the continental U.S.A.'s two largest estuaries

Nathan Hall [1]*, **Jeremy Testa** [2], **Ming Li** [3], **Hans Paerl** [1]

[1]Department of Earth Marine and Environmental Sciences, Institute of Marine Sciences, University of North Carolina at Chapel Hill, Morehead City, North Carolina, USA
[2]Chesapeake Biological Laboratory, University of Maryland Center for Environmental Science, Solomons, Maryland, USA
[3]Horn Point Laboratory, University of Maryland Center for Environmental Science, Cambridge, Maryland, USA

Abstract

In estuaries, local processes such as changing material loads from the watershed and complex circulation create dynamic environments with respect to ecosystem metabolism and carbonate chemistry that can strongly modulate impacts of global atmospheric CO_2 increases on estuarine pH. Long-term (> 20 yr) surface water pH records from the USA's two largest estuaries, Chesapeake Bay (CB) and Neuse River Estuary-Pamlico Sound (NRE-PS) were examined to understand the relative importance of atmospheric forcing vs. local processes in controlling pH. At the estuaries' heads, pH increases in CB and decreases in NRE-PS were driven primarily by changing ratios of river alkalinity to dissolved inorganic carbon concentrations. In upper reaches of CB and middle reaches of the NRE-PS, pH increases were associated with increases in phytoplankton biomass. There was no significant pH change in the lower NRE-PS and only the polyhaline CB showed a pH decline consistent with ocean acidification. In both estuaries, interannual pH variability showed robust, positive correlations with chlorophyll *a* (Chl *a*) during the spring in mid to lower estuarine regions indicative of strong control by net phytoplankton production. During summer and fall, Chl *a* and pH negatively correlated in lower regions of both estuaries, given a shift toward heterotrophy driven by changes in phytoplankton community structure and increases in the load ratio of dissolved inorganic nitrogen to organic carbon. Tropical cyclones episodically depressed pH due to vertical mixing of CO_2 rich bottom waters and post-storm terrestrial organic matter loading. Local processes we highlight represent a significant challenge for predicting future estuarine pH.

Acidification of pelagic ocean waters, or "ocean acidification," attributable to anthropogenic accumulation of atmospheric CO_2, is a well-established phenomenon (Gattuso and Hansson 2011). Although there is regionally specific variability, an estimated, annual trend of pH of approximately −0.0018 was well-constrained across most of the open ocean for the period 1981 to 2011 (Lauvset et al. 2015). Initial efforts to understand long-term trends of estuarine pH have revealed that the pH decline can be much larger than that predicted from ocean acidification (Carstensen and Duarte 2019; Cai et al. 2021), suggesting that coastal processes can exacerbate acidification. In contrast, other studies have shown that changes in watershed alkalinity inputs and nutrient-induced increases in primary production can dampen impacts from atmospheric CO_2 invasion, and even cause long-term increases in pH (Nixon et al. 2015; Carstensen and Duarte 2019; Shen et al. 2020). Thus, understanding the conflicting patterns of estuarine carbonate chemistry in response to internal changes (e.g., estuarine metabolic processes) and external forcing (e.g., atmospheric invasion of CO_2 and changes in watershed inputs) remains a challenge in estuarine systems.

Changes in pH and associated changes in calcium carbonate saturation state can have strong effects on carbon biogeochemistry, primary production, nutrient cycling, and food webs, with potential detrimental impacts on calcifying biota in both oceanic and coastal and estuarine systems (Doney et al. 2020; Glibert et al. 2022). Coastal and estuarine ecosystems provide twice the ecosystem services of open ocean ecosystems with only about a tenth of the total area (Costanza et al. 1997). The unfortunate paradox of having a poorer understanding of pH change where it likely will have the greatest immediate societal consequences has been widely recognized in the past decade (Duarte et al. 2013; Hall et al. 2020). We are now working toward a more comprehensive understanding of how increasing atmospheric CO_2 interacts with biological and watershed drivers

*Correspondence: nshall@email.unc.edu

and other system-specific characteristics (sensu Cloern 2001) to drive pH change in these highly valuable and vulnerable coastal and estuarine ecosystems (Van Dam and Wang 2019; Shen et al. 2020; Da et al. 2021).

Estuaries are also being impacted by an increasingly extreme climate system with more frequent storm-induced floods (atmospheric rivers, subtropical nor'easters, and tropical cyclones), droughts (Lehman et al., 2015; St Laurent et al. 2022), and wind events (Seneviratne et al. 2012). These drivers are known to significantly modulate biogeochemical cycling, primary and secondary production dynamics, and physical circulation patterns (Kimmel et al. 2008; Wetz and Yoskowitz 2013; Paerl et al. 2018); and in turn influence pH (Bianchi 2012; Bauman and Smith 2017). With regard to autochthonous (in system) processes, a common feature of estuarine and coastal systems is nutrient-driven eutrophication (Nixon 1995; Cloern 2001), which can promote basification through enhanced CO_2 uptake in near-surface euphotic waters, while stimulating deeper-water acidification through enhanced decomposition of newly produced organic matter (Cai et al. 2021). Estuarine susceptibility to acidification is also strongly impacted by watershed and tidal marsh export of alkalinity and organic matter which can vary substantially between estuaries due to differences in watershed geology and land use (Kaushal et al. 2013; Osburn et al. 2016; Shen et al. 2020). For some estuaries, an increasing frequency of extreme precipitation induced floods (Paerl et al. 2019), are leading to correspondingly extreme pulses of organic matter loading, which may create "hot spots" and "hot moments" (McClain et al. 2003) of organic matter decomposition and associated acidification (Letourneau and Medeiros 2019; Asmala et al. 2021).

Evaluating these interactive effects and their impacts on acidification dynamics requires long-term data sets with sufficient temporal and spatial resolution to discern the overlapping effects of short-term physical and biological drivers of pH superimposed on the effects of long-term decadal scale trends of increasing atmospheric CO_2, warming, changes in river chemistry, and eutrophication/oligotrophication patterns related to changes in nutrient loading (Baumann and Smith 2017). Here, we report on two 25 yr monthly data sets on trends in surface-water pH and linked physical–chemical parameters from the two largest estuarine complexes in the lower USA, the Chesapeake Bay (CB) and Neuse River Estuary-Pamlico Sound continuum (NRE-PS), NC. Our goals were (1) to compare the long-term acidification trends along the freshwater to marine continuum within the two estuaries and (2) to use temporal and spatial patterns of linked physical–chemical parameters to infer the relative importance of internal (autochthonous) and external (allochthonous) drivers that are modulating these trends.

Methods

The CB and NRE-PS estuarine complexes

CB and the NRE-PS system are the largest and second largest estuaries in the continental United States, respectively. These estuaries share some characteristics and have important differences in their watersheds, morphology, and circulation that shape sensitivity to drivers of pH change. CB is a ~ 300 km long drowned river valley estuary with a mean depth of 6.5 m (Table 1) that results from a narrow and deep (> 20 m) central channel flanked by broad shallow (< 10 m) shoals to the east and west. The NRE is a drowned river valley tributary estuary to PS but on average is only half as deep as CB (Table 1). PS is a bar-built lagoon with an average depth of 5 m. Two-layered estuarine circulation occurs for most of the year in both CB and the NRE (Buzzelli et al. 2002; Li et al. 2005), but PS is generally well mixed. Tides (0.5–1 m amplitude) are an important source of mixing in CB, but tides are much weaker in the NRE (< 0.1 m) and PS (0.1–0.2 m) due

Table 1. Comparison of physical and chemical properties of the CB and the NRE/PS estuary.

	Area (km²)	Volume (km³)	Tidal range (m)	Residence time (d)	Freshwater input (m³ s⁻¹)	River total alkalinity (μeq L⁻¹)	Gross primary production (g C m² yr⁻¹)
NRE	394[a]	1.3[a]	<0.1[b]	34[c]	171	367	400[a]
PS	4350[d]	21[d]	0.1–0.2[d]	365[d]	897[d]	383[j]	69[e]
CB	11,601	68	0.25–0.5[f]	180[g]	2234	1000[i]	385[h]

[a]Boyer et al. (1993).
[b]Luettich et al. (2002).
[c]Peierls et al. (2012).
[d]Giese et al. (1979).
[e]Peierls et al. (2003).
[f]Li and Zhong (2009).
[g]Du and Shen (2016).
[h]Harding et al. (2002).
[i]Shen et al. (2020) for the Susquehanna River.
[j]Calculated from flow and alkalinity data in Harned and Davenport (1990), see Supporting Information for calculation.

to the restriction of tidal flows through three narrow inlets along the North Carolina Outer Banks (Table 1). Wind is an important major driver of circulation in both CB and NRE-PS (Luettich et al. 2002; Li and Li 2011).

CB's 166,000 km² watershed includes highly agricultural areas and a growing population that is currently about 18 million people. The NRE's 14,600 km² watershed also includes rapidly urbanizing areas around the Raleigh-Durham area, and intensive agriculture (row crop and swine/poultry operations) and silviculture land use in its lower watershed (Rothenberger et al. 2009). Since the 1950s, agriculture, industry, human waste, and land use change have led to increasingly high nutrient loads for CB and NRE-PS (Harding and Perry 1997;) though with some small decreases due to nutrient management in recent decades (Paerl et al. 2014; Shen et al. 2020). Long residence times of ∼6 month for CB, ∼1 month for NRE, and 1 yr for PS (Table 1) ensures ample time for uptake of riverine nutrient loads. Consequently, the trophic status of CB and NRE-PS has increased in concert with increased nutrient inputs, particularly nitrogen, which limits phytoplankton production during the most productive summer season (Rudek et al. 1991; Harding and Perry 1997; Piehler et al. 2004). Currently, CB and NRE are eutrophic with primary production > 300 g C m^{-2} yr^{-1} (Table 1). Nutrient inputs to PS are largely assimilated in its tributary estuaries including the NRE resulting in PS being mesotrophic. In both CB and NRE, high surface layer productivity fuels oxygen demand in the bottom waters and sediment which combined with stratification leads to recurrent summertime hypoxia ($O_2 < 2$ mg L^{-1}) with high CO_2 partial pressures and low pH conditions (Crosswell et al. 2014; Cai et al. 2017). In contrast, surface waters of CB and NRE often have high oxygen, low CO_2 partial pressures and high pH by virtue of high surface water productivity rates (Crosswell et al. 2014; Cai et al. 2017). Weaker stratification and lower productivity (Table 1) generally prevents hypoxia in PS. For CB and NRE-PS, variability in river flow drives changes in residence time, salinity, and nutrient conditions that greatly affect phytoplankton productivity and community composition (Adolf et al. 2006; Peierls et al. 2012; Paerl et al. 2013).

Data sources

For CB, we analyzed monthly scale discrete measurements of observed pH, salinity, chlorophyll *a* (Chl *a*), and dissolved inorganic nutrients (nitrate + nitrite, ammonium, soluble reactive phosphate) collected since 1996 along the main stem of CB, and high-frequency pH measurements (15-min) at a select number of shallow water locations (Fig. 1). All main channel CB data were collected by the Maryland Department of Natural Resources (MDDNR), the Virginia Department of Environmental Quality, and Chesapeake Bay Program (CBP). Monthly discrete pH and Chl *a* data can be accessed through the CBP data portal (http://data.chesapeakebay.net), while high-frequency data are located at the MDDNR data portal
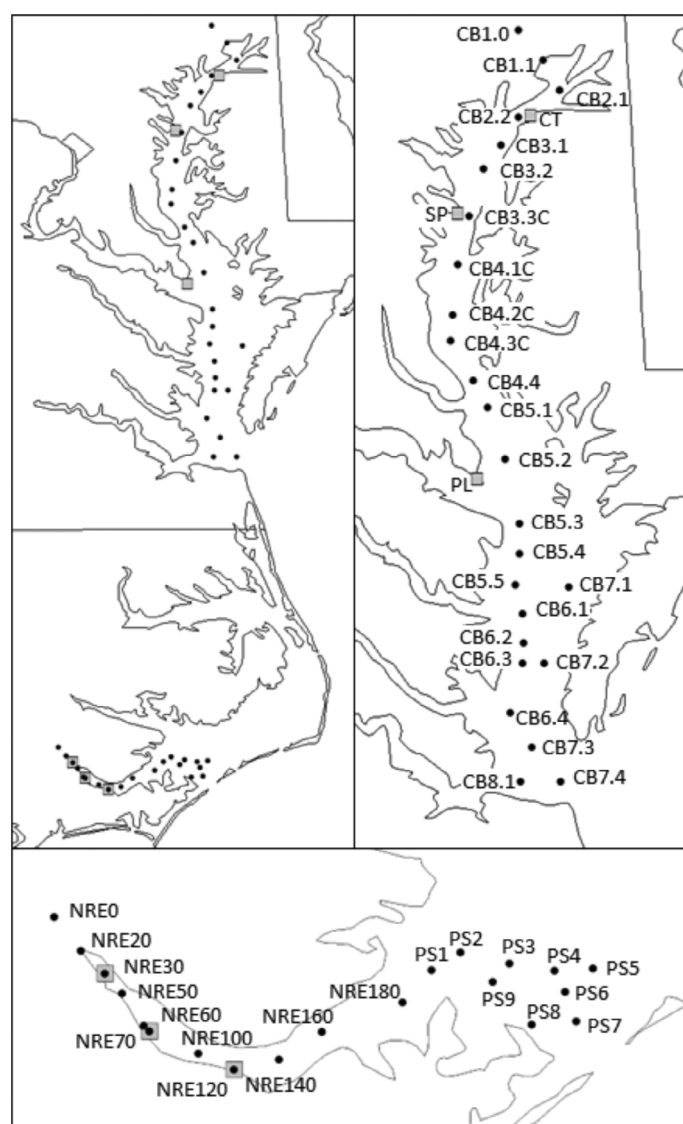
Fig. 1. Maps of long-term biweekly or monthly (black circles) and high-frequency (gray squares) monitoring stations in the CB and NRE/PS estuaries on the mid-Atlantic coast of the United States. CT, Camp Tockwogh; SP, Sandy Point; PL, Point Lookout.

(https://eyesonthebay.dnr.maryland.gov/ or available through the NOAA National Centers for Environmental Information; https://www.ncei.noaa.gov/). For the high frequency data in CB, we used an array of three research buoys (Fig. 1) that measured pH at 15 min intervals from spring (Mar–April) through early fall (Sep–Nov) of 2015–2017 for Camp Tockwogh, 2004–2007 for Sandy Point, and 2018–2020 for Point Lookout.

Loads and flow-normalized concentrations of total alkalinity, dissolved inorganic nitrogen (DIN) and total organic carbon (TOC) from the Susquehanna River were downloaded from the United States Geological Survey (USGS) River Input Monitoring Program based on monthly concentrations and daily river flow below Conowingo Dam (USGS Sta. 01578310)

and calculated using Weighted Regressions on Time Discharge and Season (Hirsch et al. 2010).

The discrete pH measures were made via vertical casts of pre-calibrated glass potentiometric electrodes at 1-m depth intervals at 3–4 week frequency between 1996 and 2020. The high frequency measures were made using the same instruments, but deployed at a fixed location (1-m from the surface) in portions of the years 2016 to 2022. Manufacturer's reported error of the pH probes throughout the study period did not exceed 0.2 and all pH measurements are reported on the NBS scale (Chesapeake Bay Program 2017). Although discrete pH measurements were made in CB since 1985, we limited our analysis window to align with the NRE-PS dataset and avoid potential measurement changes associated with different laboratories. We focused on surface pH measurements (typically 0.5 m depth) from the long-term vertical casts. We do not explicitly examine and quantify the role of air-sea CO_2 exchange on pH changes in our study, although we infer that long-term pH declines can result from oceanic or estuarine uptake of CO_2 from the atmosphere.

Accuracy of pH measurements in estuarine waters can be affected by drift and error caused by differences in the ionic strength of calibration and measurement solutions (as reasoned in Waldbusser et al. 2011). Shen et al. (2020) compared in situ pH measurements made by the CBP at three mid-bay stations (CB4.C, CB4.2C, and CB4.3C) to pH values measured from water collected at those stations and measured on board a research vessel up to 3 h later using an Orion Ross glass electrode. The two measures were highly correlated with a slope close to 1, with an absolute mean error of 0.12. The close agreement of the in situ pH sensor values with the laboratory-grade instrument provides confidence in the accuracy of the in situ measurements over the period we investigated.

For the NRE-PS, the Neuse River Estuary Modeling and Monitoring Program (ModMon) has produced a long-term (> 20 yr) database of water quality, carbonate chemistry, nutrient chemistry, phytoplankton productivity, and phytoplankton community composition observations. ModMon conducted twice monthly (1994–2020) visits to 11 mid-river stations along the NRE and approximately monthly (2000–2020) visits to nine stations in southwestern PS (Fig. 1). For this study, we only analyzed data from 1996 to 2020 due to a series of unrealistically low (~ 6) surface layer pH readings measured during 1994 and 1995. These unrealistically low pH values were also identified and eliminated from the analysis of pH conducted by Van Dam and Wang (2019).

At each station, near-surface (0.2 m) and near-bottom (0.5 m above bottom) discrete water samples were collected for laboratory analyses using a nondestructive diaphragm pump, dispensed into 4-liter polyethylene bottles, and returned to the laboratory at the University of North Carolina at Chapel Hill Institute of Marine Sciences, Morehead City, North Carolina for processing within 4 h of collection.

Hydrographic profiles of basic water quality parameters (temperature, dissolved oxygen, pH, and salinity/conductivity) were made at 0.5 m depth intervals from the surface (0.2 m depth) to 0.5 m from the bottom. All pH measurements were reported on the NBS scale. Prior to September 2000, hydrographic profiles were conducted using a multiparameter Hydrolab 3 data sonde while afterward profiles were made using a YSI 6600 sonde (Yellow Springs, Ohio, USA). Sondes were calibrated prior to each sampling trip according to the manufacturer's user's manual and had a manufacturer's declared accuracy of 0.2 (Paerl et al. 2018).

For the NRE-PS, high frequency (15 min) surface water (1 m depth) pH measurements were measured by the USGS year round from 1996 to 2009 at three stations in the NRE (02092162, 0209262905, and 0209265810) that were respectively co-located with stations NRE 30, 70, and 120. For both instruments used by ModMon and the high frequency USGS measurements, pH was measured using glass potentiometric electrodes and we assume the measurements contain a similar amount of error (+/−0.1) as observed by Shen et al. (2020) in CB when using similar glass potentiometric electrodes.

Dissolved inorganic carbon (DIC), dissolved organic carbon (DOC), particulate organic carbon (POC), nitrate/nitrite, ammonium, phosphate, and phytoplankton biomass as Chl *a* were measured from near-surface and near-bottom discrete samples. Details of analytical methods can be found in Paerl et al. (2018). Total alkalinity of the Neuse River at Sta. NRE0 was modeled with CO2SYS (Lewis and Wallace 1998) with K_1 and K_2 dissociation constants following (Cai and Wang 1998) and the $KHSO_4$ dissociation constant following Dickson et al. (1990) based on surface water measurements of DIC, pH, salinity, and temperature, and ammonium, dissolved silica, and phosphate. Loads and flow-normalized concentrations of DIN, TOC, and alkalinity were computed using weighted regressions on time discharge and season (Hirsch et al. 2010) based on concentration measurements made at the head of the NRE (Sta. NRE0) and flow measured by the USGS ~ 20 km upstream at Fort Barnwell, NC (USGS gage Sta. 02091814).

Quantifying diel pH variability

Diel cycles of pH driven by shifts in the balance of photosynthesis and respiration are strong indicators of the capacity for biological metabolism to drive estuarine pH. Daily pH cycles can also cause biases in long-term records if, for example, the time of day that samples are collected changes over the course of a monitoring program (Bauman and Smith 2017; Van Dam and Wang 2019). Such schedule changes are common within long-term monitoring programs and have occurred in both monitoring records used in this study. To quantify and remove the effect of daily pH cycles for the CB and NRE pH records, we examined existing long-term records of high frequency (15 min or higher), surface water pH data collected by autonomous data collection platforms.

For each high frequency pH record, the amplitude and phase of the diel cycle was quantified using least squares harmonic analysis, fitting high resolution pH to the function

$$pH_{est} = pH_{bar} + a\sin(2\pi(t-w)) \tag{1}$$

where pH_{est} is the modeled pH, pH_{bar} is the mean pH of the record, a is the amplitude of the diel cycle, t is time expressed as decimal days, and w is phase shift of the sine wave. To investigate how the diel cycle changed with seasonal changes of water temperature and solar radiation, estimates of the diel pH amplitude and phase were calculated for each month of the year.

Empirical model estimates of the seasonally varying diel pH cycle were used to correct pH within the long-term records to eliminate the influence of changes in the time of day that a station was sampled.

$$pH_{corr} = pH_{meas} - a\sin(2\pi(t-w)) + a\sin(2\pi(t_{ref}-w)) \tag{2}$$

where pH_{meas} is the measured pH and t_{ref} is the reference time of day within the diel cycle to which the pH measurements are corrected. The t_{ref} was chosen as 12:00 when pH was found to approximate the daily mean value. Greater detail of the methods and the results of the least square analysis of the diel pH cycle are presented in the Supporting Information.

Analysis of long-term trends

To detect long-term trends in pH, we applied a combination of traditional seasonal Kendall tests with calculation of Sen slopes to describe the direction and magnitude of secular trends (Hirsch et al. 1982), and Generalized Additive Models (GAM) (Wood, 2006) to provide a more flexible characterization of nonmonotonic patterns within the time series. Changes in Chl *a* were interpreted as changes in net phytoplankton production within the estuaries and were similarly analyzed to explore the role of changes in net phytoplankton production on pH trends.

Time series of pH obtained from the monitoring stations were analyzed using GAM as below:

$$
\begin{aligned}
y_t \sim {} & y_{t-1} + s(dnum) + s(doy) + s(sal) + ti(dnum, doy) \\
& + ti(dnum, sal) + ti(dnum, doy, sal)
\end{aligned} \tag{3}
$$

where y_t represents the response variables such as pH, y_{t-1} represents the same variables at the preceding time step to account for the autocorrelation, *dnum* is the number of months relative to the reference time (e.g., 1 for Jan 1996), *doy* is the number of months in a year (e.g., 1 for Jan), and *sal* is the monthly averaged salinity representing the influence of river flow. Among the functions used in GAM, *s*() is a smoothing function with thin plate regression splines, *ti*() represents the tensor product of two smooth functions to account for the interaction between these two variates. In Eq. 3, *s*(*dnum*)

represents the long-term residual, *s*(*doy*) represents the seasonal cycle, and *s*(*sal*) is meant to capture the effects of salinity on the interannual variations. The high-order term *ti* (*dnum, doy*) allows the seasonal cycle to change over time.

Characterizing interannual and event-scale pH drivers

Spearman rank correlations of mean monthly pH and Chl *a* were conducted to investigate how interannual variability of net primary production influenced pH during different times of the year. For example, monthly mean pH and Chl *a* values for the month of April across 25 yr were used as inputs to the rank correlation. This process was repeated for all months and for all stations along the downstream transect of each estuary. Contour plots of Spearman's *R* were used to visualize the strength and sign of the relationship across season and distance downstream.

Along the southeast and mid-Atlantic U.S. coast, tropical cyclones are important short-term events that produce extreme precipitation, storm surge, and wind impacts that can greatly impact pH. Although episodic, with rising frequencies and intensities, tropical cyclones are projected to be increasingly important drivers of biogeochemical processes in estuaries with major effects on organic C loading, spatial and temporal patterns of organic matter degradation, subsequent CO_2 formation and outgassing, all of which affect pH (Crosswell et al. 2014). Tropical cyclones also cause extreme nutrient load pulses, changes in residence time, and rapid changes in vertical stratification that affect net phytoplankton production (Paerl et al. 2018). We examined the impacts of these tropical cyclone-associated drivers and their estuarine biotic responses on pH in both estuaries. For CB, we examined Hurricane Isabel, which was a fast-moving storm that skirted the entire western shore of CB on 18 September 2003 (Li et al., 2007). While rainfall totals in the CB watershed were not extreme (< 5 cm), wind velocities out of the south exceeded 20 m s^{-1} for nearly 24 h and caused rapid destratification followed by restratification along the length of the Bay (Li et al. 2007). In the NRE-PS, Hurricane Matthew (2016) provides an example of tropical cyclone impacts from a slower moving, high precipitation storm that resulted in 100 + year flood events throughout the NRE watershed. During the flood, enhanced mobilization of terrestrial organic matter, particularly driven by connection of the river channel with floodplain wetlands, resulted in dissolved organic matter loading equivalent to 25% of the annual average in only 2 weeks following the storm (Osburn et al. 2019).

Linkages between changes in pH and net phytoplankton production following the two cyclones were examined using two approaches; one based on stoichiometry between DIC uptake and Chl *a* production and a second based on simple mixing models of water masses. First, we explored the mechanisms for a counterintuitive pH decline ($\sim$ 8.4 to 8.1) that was accompanied by a phytoplankton bloom in the mid CB region following Hurricane Isabel in 2003. Average pH decline from

~ 8.4 to 8.1 in the region was based on the mean before and after surface water H^+ concentrations at Sta. CB5.1, CB5.2, and CB5.3 where both the pH decline (Supporting Information Fig. S4) and bloom (Miller et al. 2006) were observed. The only carbonate system parameter measured prior to or after Isabel was pH, but vertical profiles of alkalinity were estimated based on salinity profiles at Sta. CB 5.1, CB 5.2, and CB 5.3 (Supporting Information Fig. S4) and using the mixing model of Cai et al. (2017); Total alkalinity = 34.676 × Salinity + 1082.7. Following Cai et al. (2017), we assumed the addition of 167 μeq kg^{-1} to subpycnocline waters (> 10 m) prior to Isabel to account for enhanced bottom-water alkalinity due to calcium carbonate dissolution, aerobic respiration, and sulfate reduction. DIC profiles were then calculated with CO2SYS. Assuming complete vertical mixing of the water column during Isabel (Li et al. 2007), poststorm alkalinity and DIC profiles were calculated via trapezoidal integration as the depth averaged alkalinity and DIC concentrations prior to the storm. Although horizontal advection and mixing were likely enhanced by the storm, horizontal gradients along the estuary are much weaker than in the vertical dimension (Li et al. 2007). Therefore, we assumed horizontal processes were negligible and vertical mixing was solely responsible for initial changes in surface water chemistry during the storm. To assess the impact on pH of DIC removal by net phytoplankton production following the storm, an assumed C : Chl *a* mass ratio of 50 (Harding et al. 2002) was multiplied by the observed increase in Chl *a* to calculate DIC consumption, which was then used to estimate the associated pH increase assuming all other parameters remained constant. As another method of determining the impact of the bloom on pH, we simulated a situation where the phytoplankton bloom failed to develop. Again assuming a 50 : 1 C : Chl *a* mass ratio, the DIC uptake necessary to form the bloom was added back to the modeled DIC during the pH minimum. CO2SYS was then used to recalculate pH under the simulated higher DIC concentration that resulted from the simulated absence of the bloom.

Second, we explored the drivers of a marked pH decline (~ 8.0 to 7.4) at Sta. NR180 following Hurricane Matthew in 2016. A mixing model of DIC (measured) and alkalinity (CO2SYS estimates based on measured DIC and pH) between Sta. NRE0 water before and during the flood with PS 3 water before the flood was used to estimate DIC and alkalinity along the salinity gradient, and CO2SYS was then used on the estimated values to calculate the pH changes that were due to conservative mixing between the two end members before and during the flood event. Although biogeochemical processes can cause alkalinity to behave nonconservatively, previous work has shown approximately conservative behavior of alkalinity following floods in the NRE (Van Dam et al. 2018). Differences between the observed pH and the pH that would have resulted from conservative mixing of DIC and alkalinity were then related to estimates of net phytoplankton production. To estimate the maximum effect of the phytoplankton production in driving the nonconservative behavior of DIC at Sta. NR180, we

assumed that the phytoplankton biomass (as Chl *a*) present on 17 October grew in situ from an initial concentration of zero within the measured water mass and that the phytoplankton DIC uptake per phytoplankton Chl *a* occurred at a 50 : 1 mass ratio (Harding et al. 2002). As another method of determining the impact of net phytoplankton production on pH, phytoplankton DIC consumption estimated from the observed post storm Chl *a* and the 50 : 1 (C : Chl *a*) stoichiometry was simply added back to the DIC observed during the pH minimum and CO2SYS was used to recalculate pH under the higher DIC concentration.

For both the CB and lower NRE storm-induced blooms, the two methods used to estimate the effect of the phytoplankton blooms on pH differ in the water chemistry simulated in the absence of a bloom due to other processes that might add or remove DIC. In particular, the effects of air sea exchange of CO_2 on pH are not accounted for in the mixing model analysis but are inherently incorporated into the analyses that simply add back DIC uptake due to the phytoplankton bloom. Thus, the differences in the simulated pH in the absence of the blooms from the two methods provides an indication of the degree to which degassing can impact pH during extreme weather events.

Results and discussion

Our analysis revealed that the CB and NRE-PS had important similarities and differences with respect to pH variability and its controls. Along the downstream axes, both estuaries have shown regionally-specific trends in pH since 1996, with long-term increases (e.g., basification) in some regions. For both estuaries, oligohaline regions were highly influenced by changing river chemistry while changes in indices of productivity were more important in driving pH change in the mesohaline and polyhaline regions. Changes in net primary production as indicated by Chl *a* covaried strongly with pH during specific seasons in both estuaries, and played a strong role in driving long-term trends across all seasons and particularly within the spring bloom. The two estuaries contrasted in their response to extreme weather events, however, where the NRE pH, salinity, and Chl *a* values were much more variable than CB.

Influence of diel cycles on long-term pH trends

The difference in trends between the raw pH records and records corrected for diel pH cycles were generally small (absolute difference < 0.02 decade^{-1}) and never changed the sign of a trend (Fig. 2a,c). This indicates that changes in sampling time of day were generally minor over the study period. However, there were a few stations in both estuaries where significant changes in sampling time of day did occur and the correction for diel pH changes significantly changed the trend magnitude. At Sta. CB5.2, there was a significant negative Seasonal Kendall test but the Sen slope for the uncorrected

data was zero (Fig. 2a). Analysis of the sampling time of day indicated a shift of sample timing from about 11:00 to 12:00 over the data record (Supporting Information Fig. S2). The corrected data record had the most extreme negative pH trend of ~ 0.06 decade^{-1} observed in CB. At Sta. PS8, the uncorrected pH record had a statistically significant trend of -0.08 decade^{-1} (Fig. 2c). The corrected pH record had a negative trend but it was statistically indistinguishable from zero. All of the other PS stations showed weak pH increases (Fig. 2c) and it appears obvious that the large negative trend in the uncorrected data is largely due to sampling bias associated with a ~ 5 h change in sampling time of day over the data record (Supporting Information Fig. S2). This change in

sampling time at Sta. PS8 resulted from PS8 being the first station sampled on each monitoring trip early (pre-2014) in the record and last later in the record. The sampling order, and therefore sampling time of day, for other stations remained consistent throughout the monitoring period. A similar magnitude of correction was applied to pH data from the CB5.2 and PS8 records despite the five-fold greater change of sampling time of day within the PS8 (Fig. 2a,c). This likely resulted from the higher magnitude of the estimated diel pH amplitude in CB (Supporting Information Fig. S1), and because the change in sampling time for CB5.2 occurred near noon when mid-day peaks in photosynthesis drive rapid changes in pH (Supporting Information Fig. S1).
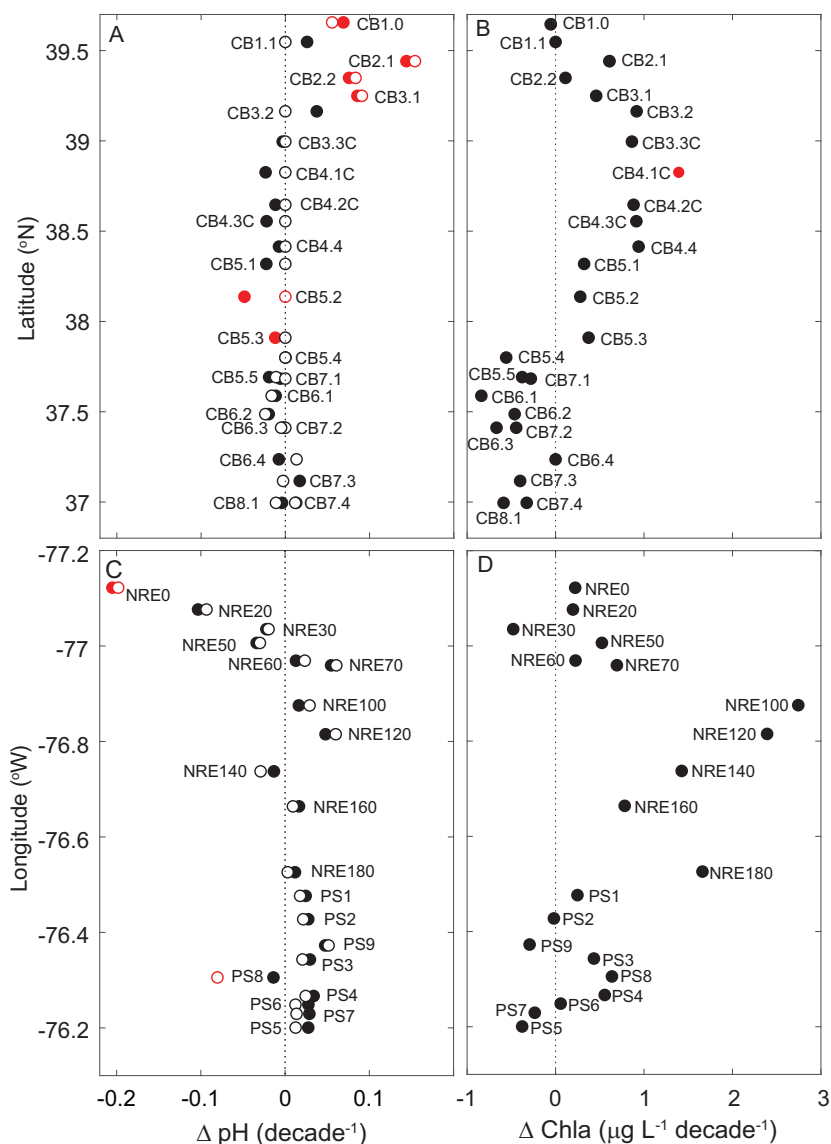
Fig. 2. Downstream patterns of Sen slopes for long-term (1996–2020) trends in pH and Chl *a* in CB (**a**, **b**) and the NRE/PS (**c**, **d**). Closed (open) symbols represent pH trends calculated using pH values that have (have not) been corrected for pH changes that result from changes in the time of day when measurements were made. Red symbols indicate statistically significant ($p < 0.05$) seasonal Kendall tests.

There is considerable uncertainty in our estimates of the diel pH cycle used to correct the data records. The high frequency records used to estimate the diel cycles in CB were short (< 1 yr long) and only covered the warmer months from April to November. For both estuaries, diel amplitudes appeared to vary along the downstream axis and the average diel amplitude from the high frequency stations may not accurately represent the diel cycle that occurred at any given station. In particular, the diel cycle is likely overestimated for the lower CB and PS where lower phytoplankton biomass and higher alkalinity would be expected to reduce diel pH excursions compared to the estuary-wide average. Nevertheless, for the stations that had large changes in the sampling time of day (e.g., PS8), any bias introduced by the correction is almost certainly smaller than the bias that occurs in the uncorrected records. Our findings support previous assertions of the importance of maintaining consistent sampling schedules or correcting for changes in sampling time of day when assessing long term changes in pH (Van Dam and Wang 2019). For the latter, maintaining high frequency monitoring buoys capable of resolving diel cycles is critical.

### Spatial patterns of long-term pH change

Long-term declines in pH, such as would be expected due to ocean acidification, were not consistently observed along the freshwater to marine gradients in the surface waters within either CB or the NRE-PS estuaries (Fig. 2). For the upper CB (Sta. CB2.1 to CB 3.2), strong increasing trends of 0.08 to 0.15/ decade were observed (Fig. 2a). Results from the GAM models show that a major increase in riverine pH occurred from the late 2000's to early 2010's coincident with a rapid increase in the ratio of riverine alkalinity to DIC (Fig. 3a,b).

The nearly identical temporal pattern of pH change in the upper estuary at Sta. CB 2.1 (Fig. 4a) indicates that riverine TA : DIC is a major influence on pH in the upper CB. Our results are consistent with previous trend analysis of historical pH data and modeling analyses that also found increasing pH in the upper estuary and primarily ascribed the pH increase to increases in Susquehanna River alkalinity relative to DIC (Shen et al. 2020; Da et al. 2021). Our analysis revealed that local increases in phytoplankton biomass (0.5–1 μg Chl a L^{-1} decade^{-1}) also likely played a role in driving increases in pH within the upper CB (Fig. 2b). This idea is further supported by strong correlations between summer pH increases and increases in Chl a described below.

In contrast to the observed pH increases in the oligohaline zone of CB, the upper stations of the NRE-PS (NRE 0 and NRE 20) showed pH declines of − 0.18 and − 0.075 decade^{-1} across the study period (1996–2020) that were much greater than can be explained by ocean acidification (Fig. 2c). These declines in pH were not accompanied by declines in Chl a (Fig. 2d), but are related to a long-term decline in the ratio of alkalinity to DIC of the freshwater carried by the Neuse River (Fig. 3d, and Van Dam and Wang 2019). GAM analyses showed that pH increased as TA : DIC increased from 1996 to the early 2000's followed by relatively stable pH and TA : DIC through ∼ 2010. After 2010, an approximate 10% decline in TA : DIC drove a nearly 0.5 decrease in pH (Fig. 3c,d). Temporal patterns of pH driven by changing TA : DIC were rapidly attenuated downstream in the estuary but could still be observed at Sta. NRE 30 as less pronounced but similarly timed pH increases in the early part (1996 to early 2000's) and decreases in the later (> 2010) part of the data record (Fig. 4c).
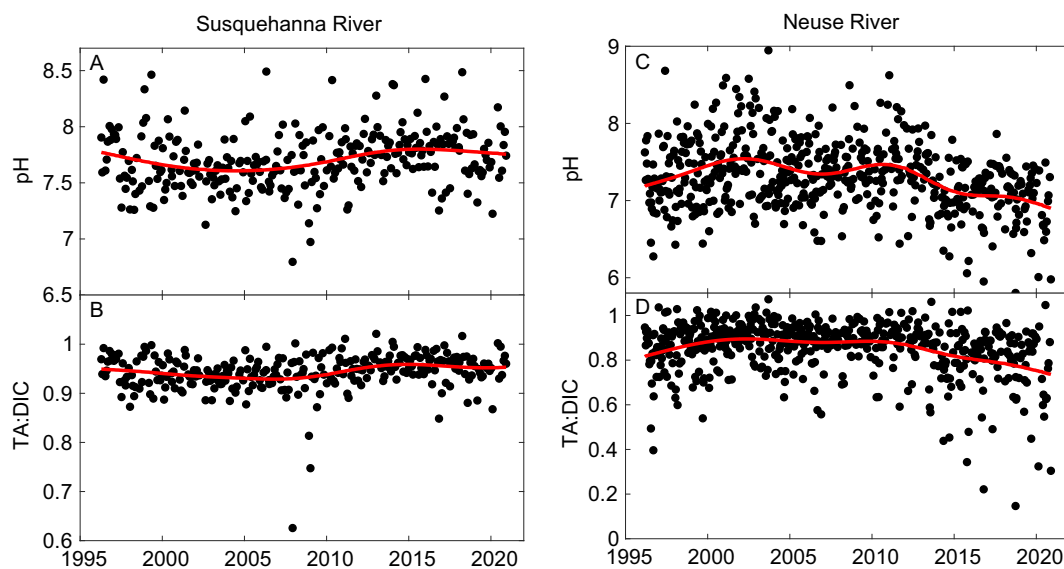
Fig. 3. Long term GAM smooths (red lines) and partial residuals (black dots) of Susquehanna (Sta. CB1.0) and Neuse River (NRE 0) pH (top panels) and TA : DIC (bottom panels).
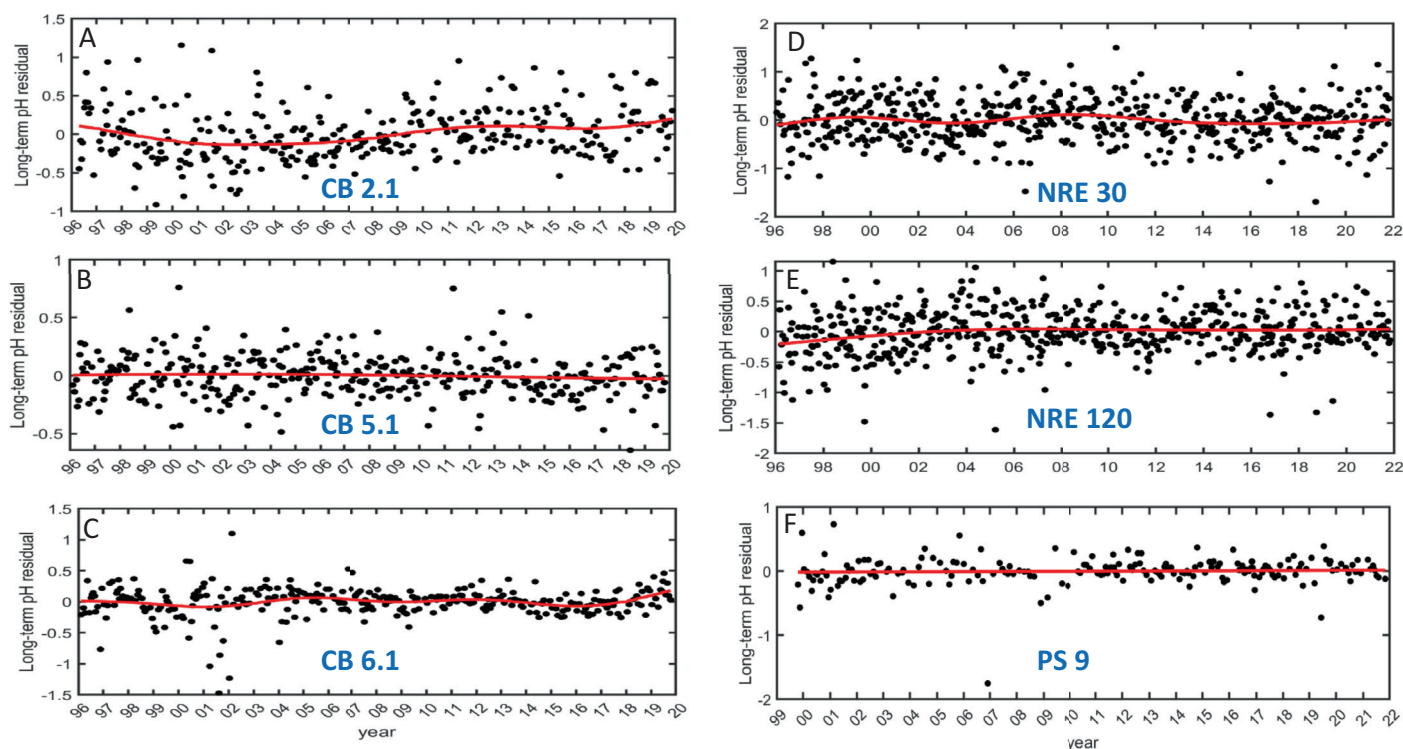
Fig. 4. GAM analyses of long term trends in surface pH at monitoring stations in CB and the NRE/PS estuaries showing the long-term smooth (red line) and partial residuals from the long-term smooth (black dots).

Thus, in both CB and NRE-PS, trends in pH at the heads of the estuaries are more responsive to changes in watershed loads of alkalinity and DIC than atmospheric CO_2 invasion or ecosystem metabolism. This may be a common theme among funnel-shaped, drowned-river estuaries where the low estuarine volume of the oligohaline zone relative to freshwater inputs creates high flushing rates (Qin and Shen 2021) that minimize the impact of planktonic metabolism in driving pH. These low-salinity zones are also rich in CO_2, leading to a predominance of outgassing (Borges and Abril 2010; Cai et al. 2017) and a minimal role of atmospheric CO_2 increases on estuarine pH. Although pH in the oligohaline zones of the two estuaries shares a strong sensitivity to riverine alkalinity : DIC ratios, the drivers of alkalinity : DIC trends are very different between the two watersheds. For the Susquehanna River, regional anthropogenic factors, particularly reduced acid mine drainage, have been implicated as the major driver of long-term increases in alkalinity : DIC and associated increases in pH (Kaushal et al. 2013). For the Neuse River, hydrology, marked by a long-term increase in river flow, is related to the decrease in alkalinity : DIC ratios (Van Dam and Wang 2019). Both alkalinity and DIC decrease with increasing flow in the Neuse River but alkalinity decreases more severely resulting in lower TA : DIC ratios under high flows (Supporting Information Fig. S3).

The mid-CB region (Sta. CB3.3 to CB5.4) exhibited weak pH declines with Sen slopes that ranged from 0 to − 0.06 per

decade and averaged −0.03 per decade. For two mid-Bay stations (CB 5.2 and 5.3) the negative trends were statistically significant (Fig. 2a). All eight mid-bay stations exhibited positive trends for Chl a of 0.5 to 1 μg L^{-1} Chl a decade^{-1}. Recent modeling analysis indicated that the observed increase in net phytoplankton production has partially offset the impacts of atmospheric invasion and negative trends in the mid-bay region would have been approximately double what was observed in the absence of the observed increased phytoplankton production (Shen et al. 2020). There has not been a definitive explanation for the observed increases in Chl a but bottom-up forcing is unlikely the cause because both Susquehanna River nitrogen loading rates and water clarity have been declining over the study period (Testa et al. 2018, 2019).

In the lower CB (Sta. CB5.5 to CB8.1), six of the ten stations showed declining, though not statistically significant trends in pH and only two stations showed weak pH increases. Long-term pH declines ranged from −0.03 to −0.005 decade^{-1}, the same order of magnitude expected from the approximate −0.02 decade^{-1} decline in oceanic pH due to ocean acidification (Lauvset et al. 2015). However, even at these downstream stations the observed pH declines cannot be solely attributed to ocean acidification because declines in phytoplankton (− 0.8 to − 0.25 μg L^{-1} Chl a decade^{-1}) were also observed at all but one of the downstream stations and modeling analyses have indicated nearly equal roles of ocean acidification and declining

phytoplankton productivity in driving the pH decline (Shen et al. 2020; Da et al. 2021).

In contrast to CB, pH trends in seaward regions of the NRE were generally positive. Below Sta. NRE 50, 16 of the 17 stations showed increasing trends in pH that ranged from 0.005 to 0.07 decade^{-1}. Although the seasonal Kendall test found that none of these individual trends were statistically significant, the probability of such a high proportion (16/17) of positive trends when the true proportion is split evenly is exceedingly low ($\chi^2 = 8.34$, $p = 0.004$) which provides confidence in a positive pH trend for the lower region of NRE/ PS. In the mesohaline zone of the NRE, increases in Chl a ranging from ~ 1–3 μg L^{-1} decade^{-1} suggest that eutrophication was likely responsible for observed pH increases. Efforts to reduce Neuse River nutrient loads in the 1980's-1990's were highly successful but nitrogen loads have since increased (Strickling and Obenour 2018) and likely are responsible for observed Chl a increases. Farther downstream in PS, consistent increases in pH of ~ 0.02 decade^{-1} cannot be explained solely based on changes in net production because stations were split nearly evenly between small increases and decreases of Chl a. The positive pH trend for much of the NRE-PS also contrasts with the consistent negative trends of surface water pH described by Van Dam and Wang (2019). The discrepancy is likely due to the longer, 24-yr record used in this study compared to Van Dam and Wang's 12-yr (2005–2017) record which as mentioned previously was a period marked by strong decreases in TA : DIC ratios related to increasing river discharge (Van Dam and Wang 2019).

Primary productivity as a driver of interannual pH variability

Spatial and seasonal variability in the interannual correlation between Chl a and pH indicated strong differences in the extent that primary productivity and community respiration are coupled in the two estuaries. The strongest positive interannual correlations between Chl a and pH occurred during the spring bloom in both systems (Fig. 5a,b), February to April in the NRE-PS (Pinckney et al. 1998) and from late March to early May in CB (Harding et al. 2002). Positive relationships between Chl a and pH arise when respiration is temporally or spatially decoupled from primary productivity to create net autotrophic conditions. At temperate latitudes, net autotrophy of surface waters in spring is common (Carstensen and Duarte 2019) because much of the respiration of the spring bloom organic matter occurs in bottom waters later in summer (Carstensen and Duarte 2019). In both estuaries, the intensity of the spring bloom is strongly regulated by the dual roles of river flow in delivering nutrients and flushing effects on phytoplankton biomass (Harding et al. 2002; Katin et al. 2021). In CB, the spring bloom was most intense when high flows in late winter led to strong nutrient loading followed by low flows during spring, which allowed sufficiently long residence time for phytoplankton biomass to develop (Harding et al. 2002). In years when flow provides sufficient nutrients and allows time for phytoplankton growth, high phytoplankton productivity should drive increases in pH and produce the strong observed correlations between pH and Chl a during the spring bloom period (Fig. 5b). Spatially, the positive association between interannual pH and Chl a variability during the spring bloom was strongest in the mesohaline region (-76.6 to $-77.0°$W), which as noted above has a sufficiently long residence time to allow phytoplankton assimilation of riverine nutrient loads.

In summer, the zone of strong positive interannual correlation between Chl a and pH occurred in the oligohaline zone of the two estuaries where it remained before migrating back
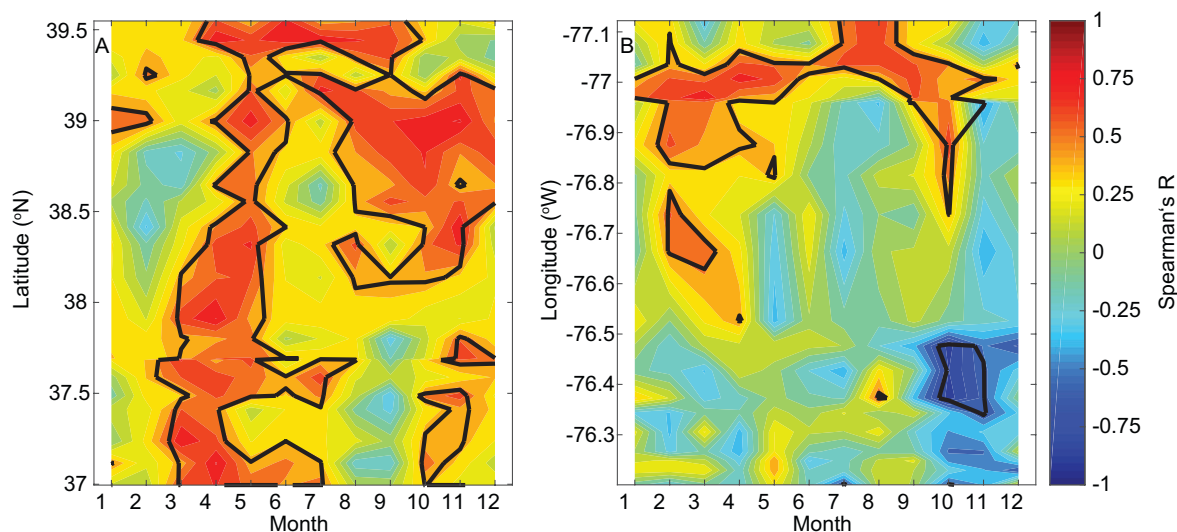
Fig. 5. Spearman's rank correlation between monthly surface pH and Chl a in CB (**a**) and the NRE/PS estuaries (**b**). Black lines indicate contours of statistically significant correlations ($p < 0.05$).

downstream to the mesohaline region in fall (Fig. 5a,b). The oligohaline zones of these estuaries are generally nutrient rich. However, net phytoplankton production in the oligohaline zones of both estuaries is highly dynamic and strongly dependent on river flow which governs flushing losses and light availability due to levels of suspended sediment (Peierls et al. 2012; Qin and Shen 2021). Under low flow conditions that often occur in summer, weak flushing and high light availability promote net phytoplankton production while higher summer flows stifle net production in the oligohaline zone. The strong observed positive correlation of pH and Chl *a* in this zone during summer is likely due to alternations between these bloom/non-bloom conditions as downstream transport and sedimentation of organic matter in these highly advective and stratified zones spatially decouples production and respiration. The positive relationship in the oligohaline zone (Fig. 5a,b) of the NRE is likely also enhanced by the higher alkalinity to DIC ratio of river water under low river flow conditions (Supporting Information Fig. S3).

In the mesohaline and polyhaline zones during summer, interannual correlations between pH and Chl *a* were weaker than other regions and seasons in both estuaries, and in the NRE-PS were generally negative (Fig. 5a,b). The contrasting lack of correlation between pH and Chl *a* during summer in the mesohaline and polyhaline regions and strong correlations in spring are likely related to nutrient availability and temperature which tend to couple production and respiration in summer and decouple production and respiration in spring. Due to rapid nutrient uptake upstream, the mesohaline and polyhaline regions of these two estuaries are strongly nutrient limited during summer (Rudek et al. 1991; Piehler et al. 2004; Zhang et al. 2021). Under nutrient limited conditions, the phytoplankton community shifts from the spring bloom dominated largely by diatoms to a mix of flagellates that are largely mixotrophic and picoplankton well adapted to low nutrients (Adolf et al. 2006; Gaulke et al. 2010; Paerl et al. 2013). Most of the summer production is cycled within the microbial loop so that export of photosynthetically produced organic matter from the surface layer is minimal and production is closely balanced by respiration with a reduced impact on pH compared to spring when net ecosystem metabolism and organic matter export is high (e.g., Kemp et al. 1997; Testa and Kemp 2008).

Seasonal differences in the correlations between pH and Chl *a* in both systems are also likely driven by differences in the composition of inflowing rivers. In the lower parts of both estuaries, summer and fall net phytoplankton production is nitrogen limited (Paerl et al. 2014; Zhang et al. 2021). Significant pulses of DIN that stimulate summertime net phytoplankton production in these areas are usually also accompanied by high watershed inputs of organic matter that can fuel bacterial respiration (Peierls and Paerl 2010). At the ecosystem level, the ratio of DIN : TOC has been shown to be a strong predictor of net ecosystem metabolism (Kemp et al. 1997). DIN : TOC from the Susquehanna and Neuse Rivers exhibits a significant seasonal pattern with higher DIN : TOC during winter and spring and lower DIN : TOC during summer and fall (Fig. 6). High summer temperatures stimulate respiration to a greater degree than phytoplankton production (Harris et al. 2006). The combination of high summer temperatures and higher relative levels of resource availability for heterotrophs vs. phytoplankton likely causes the effect of enhanced phytoplankton production on pH to be overwhelmed by bacterial respiration. Hence bloom formation can occur under net heterotrophic conditions and cause the observed negative relationships between Chl *a* and pH during summer in the lower parts of these estuaries. In both systems, the lowest DIN : TOC ratios are also associated with high flows such that the highest nutrients loads but also the lowest DIN : TOC load ratios occur during summer/fall floods. In many cases, these summer/fall flood events are associated with tropical cyclones (Fig. 6b,d).

Effects of extreme weather events

The impacts of Hurricane Isabel on CB pH were primarily driven by wind-induced mixing of the water-column and its impact on net phytoplankton production. Mixing of higher salinity bottom water into the surface layer was evident in CB following Isabel as increases in surface water salinity following Isabel's passage in the oligohaline and mesohaline zones of CB (CB3.1, CB4.3C, and CB5.3 in Fig. 7a) where stratification prior to the storm was strong (Li et al. 2007). Prior to the storm, unusually high summer river flows during the summer of 2003 fueled higher than average primary production and the freshening of the surface layer enhanced vertical stratification in the mid Bay region (Miller et al. 2006). The combination of high rates of organic matter oxidation and strong stratification in the mid Bay led to hypoxic bottom waters with low pH (7.4–7.5) for the mid Bay region (Supporting Information Fig. S4). During Isabel, vertical mixing resulted in rapid declines of 0.2 to 0.3 in surface water pH (Fig. 7b, Supporting Information Fig. S4). The mixing of ammonium to the surface stimulated a well-documented, diatom bloom in the mid Bay region from 37.2°N to 87.4°N (Miller et al. 2006) (CB5.3 in Fig. 7c). Average phytoplankton biomass increased by $\sim 50\%$ from 8.7 to 13.4 μg L^{-1} within the bloom region (CB5.3 in Fig. 7c; Fig. 1 in Miller et al. 2006) but the production by the bloom did not offset the decline in pH. The lower Bay (CB8.1) did not appear strongly impacted by Isabel.

In contrast to Hurricane Isabel in CB, Hurricane Matthew in the NRE-PS was primarily associated with extreme freshwater inflows and associated watershed materials. Salinity dropped to near zero throughout the NRE and from > 17 to ~ 10 in PS (Fig. 7d). Respiratory CO_2 inputs fueled by the huge load of organic rich, freshwater caused rapid declines in pH that ranged from a drop of almost 1 at the most upstream stations (NRE70 and 120) to ~ 0.3 in PS (Fig. 7e). Net phytoplankton production was displaced in the upper estuary due
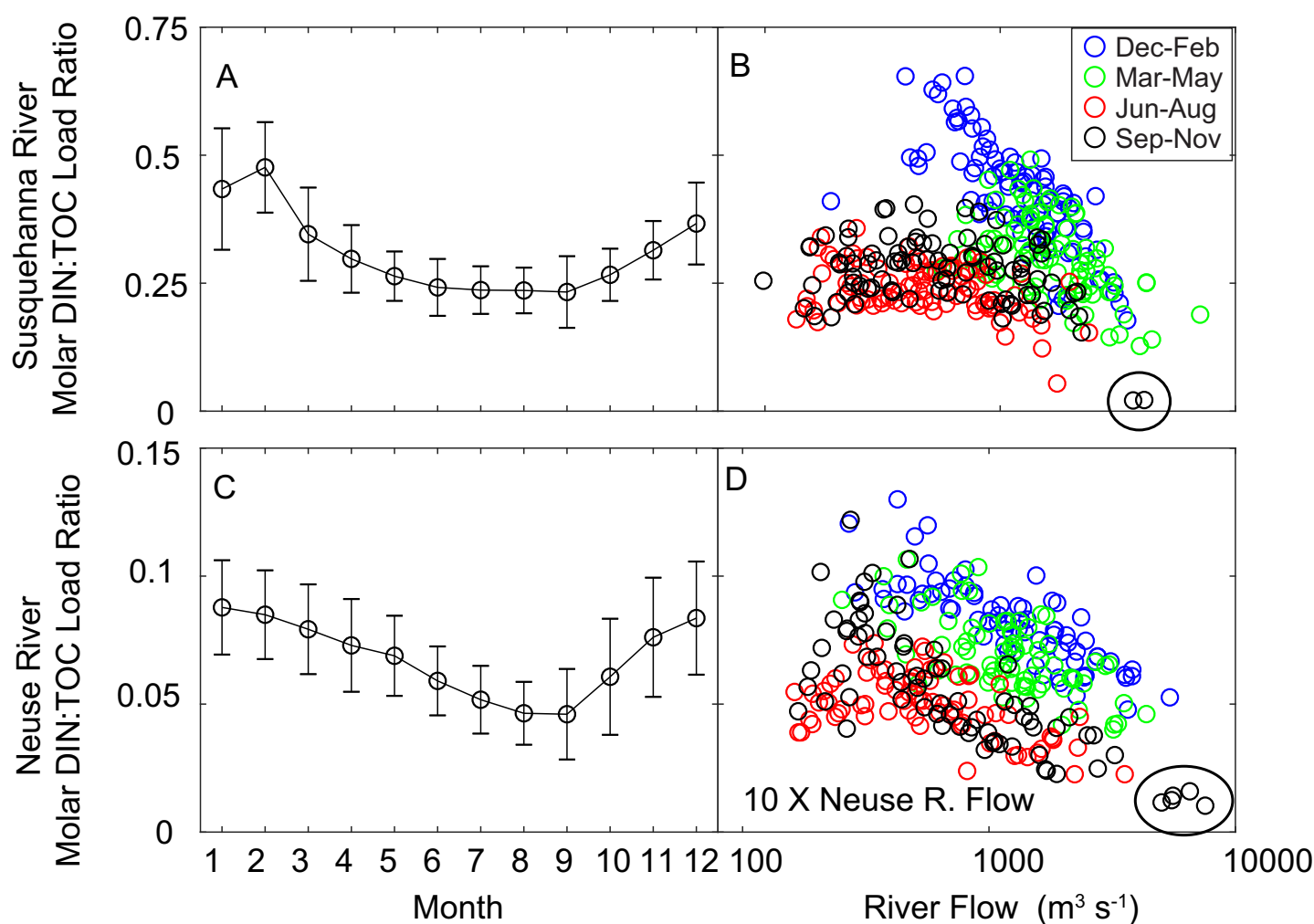
Fig. 6. Seasonal and flow-related variability in load ratios for DIN : TOC for the Susquehanna River and Neuse River modeled using WRTDS. Left panels (**a, c**) show the arithmetic mean and standard deviation of DIN : TOC loads for each month of the year. Right panels (**b, d**) show the ratio of monthly averaged DIN and TOC loads vs. monthly averaged river flow during the study period. The two lowest monthly average DIN : TOC ratios for the Susquehanna River are circled and are associated with Hurricane Ivan (Sep 2004), and Hurricane Irene/Tropical Storm Lee (Sep 2011) ordered lowest to highest. The five lowest monthly average DIN : TOC ratios for Neuse River are circled and are associated with Hurricanes Floyd (Sep 1999), Florence (Sep 2018), Fran (Sep 1996), Matthew (Oct 2016) and Floyd/Irene (Oct 1999) ordered from lowest to highest DIN : TOC.

to rapid flushing but was stimulated by high nutrient loads in the lower estuary at Sta. NRE180 and PS (Fig. 7f).

Thus, in both mid-CB and lower NRE-PS systems, phytoplankton blooms that followed storms were accompanied by decreases rather than increases in pH. Mechanisms behind these counterintuitive storm impacts were explored using a combination of mixing model analyses and stoichiometric considerations. First, we explored the drivers of the pH decline ($\sim$ 8.4–8.1) in the mid CB region where an increase of $\sim$ 5 μg L^{-1} Chl a was observed following Hurricane Isabel. A mixing model that accounted for complete vertical mixing of the prestorm DIC and alkalinity profiles (see methods for details) indicated that DIC inputs into the surface layer during mixing by Isabel should have caused pH to decrease $\sim$ 0.5 units from $\sim$ 8.4 to 7.9 (Fig. 8a). Assuming a 50 : 1 mass

ratio of DIC uptake per unit Chl a increase, a DIC consumption of about 250 μg C L^{-1} (21 μmol L^{-1}) was used to estimate an $\sim$ 0.1 unit pH increase caused by the ammonium stimulated bloom.

As another method of determining the impact of the bloom on pH, the DIC consumption of the bloom was simply added back to the modeled DIC during the pH minimum and CO2SYS was used to recalculate pH under the higher DIC concentration. Using this method, bloom production was estimated to elevate pH by $\sim$ 0.08 units (Fig. 8a). Both approaches reveal that the magnitude of the bloom stimulated by ammonium mixed into the surface layer was insufficient to overcome the effects of DIC inputs in driving the surface water pH decline.

Second, we explored the drivers of the pH decline ($\sim$ 8.0–7.4) at Sta. NR180 where a phytoplankton bloom of 30 μg L^{-1}
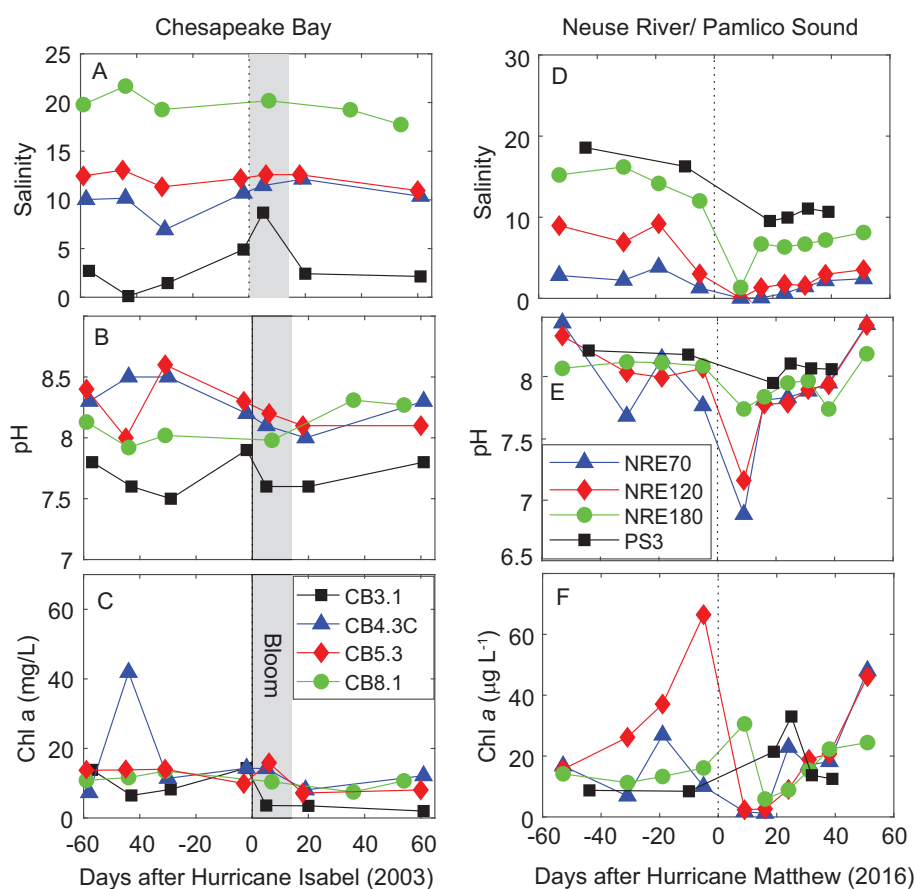
Fig. 7. Time-series of salinity (top panels), pH (middle panels), and Chl *a* (lower panels) in the 60 d before and after the passage of Hurricane Isabel (left panels, 2003) at four stations in CB and Hurricane Irene (right panels, 2011) at four stations in the NRE/PS.

Chl *a* was observed following Hurricane Matthew (Fig. 7f). Calculations of pH based on conservative mixing of alkalinity and DIC from the head of the estuary before and after Hurricane Matthew with pre-Matthew waters from PS very closely approximated pH at Sta. NR180 prior to Matthew, but during the flood event underestimated the observed pH by ~ 1.2 (Fig. 8b). Assuming that all $30 \, \mu g \, L^{-1}$ of the phytoplankton biomass grew in situ within the water mass present on 17 October and a C : Chl *a* mass ratio of 50 (Harding et al. 2002), DIC consumption was $\sim 1500 \, \mu g \, L^{-1}$ ($125 \, \mu mol \, L^{-1}$) due to the bloom. Subtracting off the DIC consumption by the bloom from the DIC estimated at NR180 using the mixing model accounted for ~ 1 pH unit of the ~ 1.2 unit underestimate of pH based only on conservative mixing (Fig. 8b). Adding back the DIC uptake by the bloom to the DIC concentration observed during the pH minimum and then recalculating pH at the higher DIC concentration showed that the bloom elevated pH by ~ 0.8 units, similar in magnitude to the impact on pH estimated from the mixing model analysis (Fig. 8b).

For both CB and NRE, after accounting for DIC uptake by the blooms and conservative mixing of the water column or estuarine end members, there was still a 0.1 and 0.25 unit pH

difference, respectively, between observed and estimated pH. Following these storms, intense degassing of CO_2 alleviates part of the potential pH decrease (Crosswell et al. 2014), and the lack of accounting for degassing in the conservative mixing models may explain much of the underestimation of pH in the mixing models compared to the observed pH (Fig. 8a,b). Our ability to assess the full impacts of such extreme events on the estuarine carbonate system is limited because there are potentially important transient storm effects like degassing that we cannot capture with the available data.

The accuracy of our estimates of DIC uptake by the blooms, and thus impact on pH, in both systems relies on the accuracy of the assumed 50 : 1 phytoplankton C : Chl *a* ratio. The C : Chl *a* ratio of phytoplankton can vary between ~ 20 and 400 with the extreme low and high values associated with severe light and nutrient limitation, respectively (Cloern 2001). We tested a range of possible C : Chl *a* ratios and found that for the case of the bloom following Hurricane Isabel in CB, the phytoplankton C : Chl *a* ratio of would have to be ~ 300 for phytoplankton DIC uptake to maintain a pre-storm pH. For the NRE case following Hurricane Matthew, the $31 \, \mu g \, L^{-1}$ increase in Chl *a* with a C : Chl *a* ratio of 65 would draw down enough DIC to maintain a
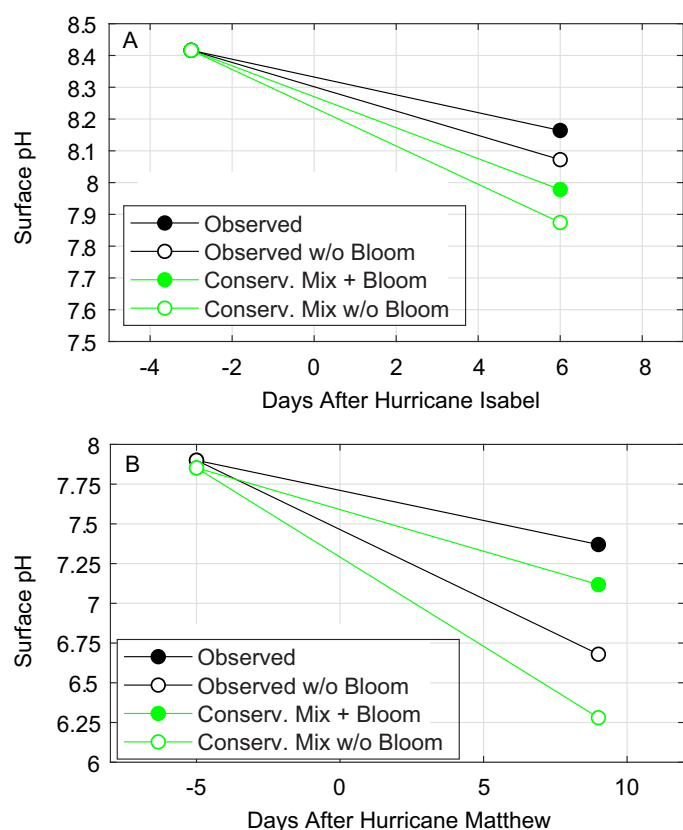
Fig. 8. Modeled impacts of phytoplankton blooms on surface water pH following Hurricane Isabel in the mid CB region, and Hurricane Matthew in the lower NRE. For panel A, "Observed" values are based on the regional average surface water H^+ concentration for the mid-CB region. For panel B, "Observed" values are the observed surface water pH of NRE Sta. NR180. "Conserv. Mix w/o Bloom" are values derived from (Panel A) conservative mixing of the pre-storm vertical profiles of DIC and alkalinity or (Panel B) conservative mixing of the prestorm and poststorm riverine DIC and alkalinity with prestorm DIC and alkalinity from PS Sta. PS3. "Observed w/o Bloom" scenarios were calculated based on the "Observed" condition with DIC added to simulate the absence of DIC uptake by phytoplankton production. "Conserv. Mix + Bloom" scenarios were calculated based on values from "Conserv. Mix w/o Bloom" with DIC removed to simulate DIC drawdown by phytoplankton production.

prestorm pH. For either case, there is good evidence that the real C : Chl *a* ratio during the blooms was almost certainly lower than what would be required for the blooms to remove enough DIC to prevent a decrease in pH. First, for the CB case, a C : Chl *a* ratio of ~ 300 has only been observed under high light and extreme nutrient starved growth conditions (Cloern et al. 1995). Availability of growth-limiting ammonium was high following the mixing event (Miller et al. 2006), and light availability, even under normal, non-post storm conditions, is not high in the mid CB region (Harding et al. 2002). For the case of the NRE, the measured molar ratio of POC to Chl *a* within the bloom waters was only 54, and certainly some fraction of the carbon occurred in pools other than phytoplankton. Thus, realistic changes to the C : Chl *a* ratio used in these analyses would not change the

conclusion that the impact of post storm blooms on surface water pH is overwhelmed by the impact of extremely high CO_2 inputs in depressing pH.

The origin of CO_2 enriched waters following large storms can be bottom waters that accumulate CO_2 from organic matter degradation as was seen during Hurricane Isabel in CB, or the watershed where flushing of soil pore waters directly contributes high CO_2 and indirectly contributes to high CO_2 through extreme loading of organic matter to estuaries (Crosswell et al. 2014; Van Dam et al. 2018). In the NRE, extreme organic loading is believed to result from floodwaters connecting to wetlands within the flood plain (Rudolf et al. 2020). Simultaneously, flood waters from tropical cyclones dilute DIN levels (Paerl et al. 2018). Thus, tropical cyclones which occur during warm weather and produce the highest levels of discharge to the Neuse River represent the extremes of conditions that cause low DIN : TOC load ratios. In fact, the lowest observed DIN : TOC load ratios have occurred during the extreme flooding from Hurricanes Floyd, Matthew, and Florence. We hypothesize that inputs of CO_2, organic matter, and nutrients from tropical cyclones play a large role in driving the strong negative relationship observed between interannual variability in surface water Chl *a* and pH in the polyhaline region of the NRE (Fig. 5b). The greater expression of this tropical cyclone-related phenomena in the NRE-PS than in CB may relate to the larger size of CB and its watershed. Given a typical tropical cyclone diameter of ~ 200 km (Guo and Matyas 2016), a small watershed like the Neuse River could be almost completely covered by a tropical cyclone while only a small fraction of the much larger CB watershed would be impacted. Thus, tropical cyclone effects on watershed delivery of CO_2, organic matter, and nutrients on the main stem of a large estuary like the Chesapeake would be significantly dampened by large unimpacted areas of the watershed.

Summary and conclusions

Estuarine acidification is a complex phenomenon influenced by temporal and spatial patterns in hydrology and productivity that result from inputs of nutrients and inorganic carbon from their watersheds. Our comparison of the differential long-term patterns of pH in two large ecosystems reveals both consistencies and discrepancies in spatial patterns of trend, but comparable, diverse driving factors. Although long-term trends were relatively weak in both estuaries, the trends reflect a response to a combination of altered watershed chemistry (CB and NRE-PS), primary productivity (CB and NRE-PS), and an ocean acidification signal for the lower region of CB. Both systems are responsive to the carbonate chemistry in inflowing rivers in their upstream reaches, but the Susquehanna River (CB) is becoming more alkaline while the Neuse (NRE-PS) is becoming more acidic. The ocean acidification signal of the lower CB contrasts with the basification of the most marine influenced regions of the lagoonal NRE-PS system, which have limited exchange with coastal waters and may be

less vulnerable to acidification. The coastal end members of both estuaries have experienced similar pH declines due to ocean acidification (Xu et al. 2020) and the difference in pH trends of the downstream regions of both estuaries underscores the important role that differences in hydrological connectivity can play in shaping estuarine pH responses to similar regional-scale forcing. Long-term trends were detectable despite substantial diel variability in pH resulting from high estuarine productivity in both systems, which is much larger than the scale of global pH declines associated with atmospheric CO_2 invasion. While our results are relevant for productive surface waters, they are not necessarily relevant for bottom waters in stratified systems like CB, where bottom-water pH would be reduced by eutrophication (Cai et al. 2017; Shen et al. 2020) given that these waters essentially receive excess organic matter from the surface water that is respired to generate CO_2. Tropical storm events are more clearly associated with pH variability in the NRE-PS Neuse than in CB, given the larger impact of tropical storms and small watershed size relative to storm size in the NRE-PS, driving higher vulnerability. Thus, future changes in watershed chemistry and productivity will complicate the detection of an acidification effect in estuarine environments.

Data availability statement

The data used in this analysis are publicly available and reported as part of long-term monitoring programs. Data for watershed discharge, river chemistry, water-column pH and chlorophyll *a* concentrations, and high-frequency records of pH are available from federal and state agencies: United States Geological Survey, Chesapeake Bay Program, Maryland Departments of Natural Resources (DNR) and Environment (MDE). Data collected by the Neuse River Modeling and Monitoring (ModMon) program can be accessed through the Southeast Coastal Ocean Observing Regional Association's data portal at https://portal.secoora.org/.

References

Adolf, J. E., C. L. Yeager, W. D. Miller, M. E. Mallonee, and L. W. Harding Jr. 2006. Environmental forcing of phytoplankton floral composition, biomass, and primary productivity in Chesapeake Bay, USA. Estuar. Coast. Shelf Sci. **67**: 108–122.

Asmala, E., C. L. Osburn, R. W. Paerl, and H. W. Paerl. 2021. Elevated organic carbon pulses persist in estuarine environment after major storm events. Limnol. Oceanogr. Lett. **6**: 43–50. doi:10.1002/lol2.10169

Baumann, H., and E. Smith. 2017. Quantifying metabolically-driven pH and oxygen fluctuations in US nearshore habitats at diel to interannual time-scales. Estuaries Coast **41**: 1102–1117.

Bianchi, T. S. 2012. Estuarine chemistry. *In* J. D. Day, B. C. Crump, W. M. Kemp, and A. J. Aranciba [eds.], Estuarine

ecology. Wiley Online Library. doi:10.1002/9781118412787.ch3

Borges, A. V., and G. Abril. 2010. Carbon dioxide and methane dynamics in estuaries, p. 119–161. Chapter 4. *In* E. Wolanski and D. McLusky [eds.], Treatise on estuarine and coastal science-volume 5: Biogeochemistry. Academic Press.

Boyer, J. N., R. R. Christian, and D. W. Stanley. 1993. Patterns of phytoplankton primary productivity in the Neuse River estuary, North Carolina, USA. Mar. Ecol. Prog. Ser. **97**: 287–297.

Buzzelli, C. P., R. A. Luettich Jr., S. P. Powers, C. H. Peterson, J. E. McNinch, J. L. Pinckney, and H. W. Paerl. 2002. Estimating the spatial extent of bottom-water hypoxia and habitat degradation in a shallow estuary. Mar. Ecol. Prog. Ser. **230**: 103–112.

Cai, W. J., and Y. Wang. 1998. The chemistry, fluxes, and sources of carbon dioxide in the estuarine waters of the Satilla and Altamaha Rivers, Georgia. Limnol. Oceanogr. **43**: 657–668. doi:10.4319/lo.1998.43.4.0657

Cai, W.-J., and others. 2017. Redox reactions and weak buffering capacity lead to acidification in the Chesapeake Bay. Nat. Commun. **8**: 369. doi:10.1038/s41467-017-00417-7

Cai, W. J., and others. 2021. Natural and anthropogenic drivers of acidification in large estuaries. Ann. Rev. Mar. Sci. **13**: 23–55. doi:10.1146/annurev-marine-010419-011004

Carstensen, J., and C. M. Duarte. 2019. Drivers of pH variability in coastal ecosystems. Environ. Sci. Tech. **53**: 4020–4029.

Chesapeake Bay Program. 2017. Methods and quality assurance for Chesapeake Bay water quality monitoring programs. Chesapeake Bay Program.

Cloern, J. E. 2001. Our evolving conceptual model of the coastal eutrophication problem. Mar. Ecol. Prog. Ser. **210**: 223–253.

Cloern, J. E., C. Grenz, and L. V. Lucas. 1995. An empirical model of the phytoplankton chlorophyll: carbon ratio- the conversion factor between productivity and growth rate. Limnol. Oceanogr. **40**: 1313–1321.

Costanza, R., and others. 1997. The value of the world's ecosystem services and natural capital. Nature **387**: 253–260.

Crosswell, J. R. M. S., B. H. Wetz, and H. W. Paerl. 2014. Extensive CO_2 emissions from shallow coastal waters during passage of hurricane Irene (august 2011) over the mid-Atlantic Coast of the U.S.A. Limnol. Oceanogr. **59**: 1651–1665.

Da, F., M. A. M. Friedrichs, P. St-Laurent, E. H. Shadwick, R. G. Najjar, and K. E. Hinson. 2021. Mechanisms driving decadal changes in the carbonate system of a coastal plain estuary. J. Geophys. Res. Ocean **126**: e2021JC017239. doi:10.1029/2021JC017239

Dickson, A. G., D. J. Wesolowski, D. A. Palmer, and R. E. Mesmer. 1990. Dissociation constant of bisulfate ion in aqueous sodium chloride solutions to 250°C. J. Phys. Chem. **94**: 7978–7985. doi:10.1021/j100383a042

Doney, S., D. S. Busch, S. R. Cooley, and K. J. Kroeker. 2020. The impacts of ocean acidification on marine ecosystems and reliant human communities. Ann. Rev. Environ. Resourc. **45**: 11.1–11.30.

Du, J., and J. Shen. 2016. Water residence time in Chesapeake Bay for 1980-2012. J. Mar. Syst. **164**: 101–111. doi:10.1016/j.jmarsys.2016.08.011

Duarte, C. M., I. E. Hendriks, T. S. Moore, Y. S. Olsen, A. Steckbauer, L. Ramajo, J. Carstensen, J. A. Trotter, and M. McCulloch. 2013. Is ocean acidification an open-ocean syndrome? Understanding anthropogenic impacts on seawater pH. Estuaries Coast **36**: 221–236. doi:10.1007/s12237-013-9594-3

Gattuso, J. P., and L. Hansson [eds.]. 2011. Ocean acidification. Oxford University Press.

Gaulke, A. K., M. S. Wetz, and H. W. Paerl. 2010. Picophytoplankton: A major contributor to planktonic biomass and primary production in a eutrophic, river-dominated estuary. Estuar. Coast. Shelf Sci. **90**: 45–54. doi:10.1016/j.ecss.2010.08.006

Giese, G. L., H. B. Wilder, and G. G. Parker Jr. 1979. Hydrology of major estuaries and sounds of North Carolina. U.S. Geological Survey Water Supply Paper 2221. U.S. Government Printing Office.

Glibert, P. M., W. Cai, E. R. Hall, M. Li, K. L. Main, K. A. Rose, J. M. Testa, and N. K. Vidyarathna. 2022. Stressing over the complexities of multiple stressors in marine and estuarine systems. Ocean-Land-Atmosphere Res **2022**: 9787258. doi:10.34133/2022/9787258

Guo, Q., and C. J. Matyas. 2016. Comparing the spatial extent of Atlantic basin tropical cyclone wind and rain fields prior to land interaction. Phys. Geogr. **37**: 5–25.

Hall, E. R., and others. 2020. Acidification in the U.S. southeast: Causes, potential consequences and the role of the Southeast Ocean and coastal acidification network. Frontier Mar. Sci. **7**: 548. doi:10.3389/fmars.2020.00548

Harding, L. W., and E. S. Perry. 1997. Long-term increase of phytoplankton biomass in Chesapeake Bay, 1950-1994. Mar. Ecol. Prog. Ser. **157**: 39–52.

Harding, L. W., M. M. Mallonee, and E. S. Perry. 2002. Toward a predictive understanding of primary productivity in a temperate, partially stratified estuary. Estuar. Coast. Shelf Sci. **55**: 427–463.

Harned, D. A., and M. S. Davenport. 1990. Water-quality and basin activities and characteristics for the Albemarle-Pamlico estuarine system, North Carolina and Virginia. Open-file Report 90-398. U.S. Geological Survey.

Harris, L. A., C. M. Duarte, and S. W. Nixon. 2006. Allometric laws and prediction in estuarine and coastal ecology. Estuaries Coast **29**: 340–344.

Hirsch, R. M., J. R. Slack, and R. A. Smith. 1982. Techniques of trend analysis for monthly water quality data. Water Resour. Res. **18**: 107–121.

Hirsch, R. M., D. L. Moyer, and S. A. Archfield. 2010. Weighted regressions on time, discharge, and season (WRTDS), with an application to Chesapeake Bay river inputs. J. Am. Water Resour. Assoc. **46**: 857–880.

Katin, A., D. Del Giudice, N. S. Hall, H. W. Paerl, and D. R. Obenour. 2021. Simulating algal dynamics within a Bayesian framework to evaluate controls on estuary productivity. Ecol. Model. **447**: 109497. doi:10.1016/j.ecolmodel.2021.109497

Kaushal, S. S., G. E. Likens, R. M. Utz, M. L. Pace, M. Grese, and M. Yepsen. 2013. Increased river alkalinization in the eastern U.S. Environ. Sci. Technol. **47**: 10302–10311. doi:10.1021/es401046s

Kemp, W. M., E. M. Smith, M. Marvin-DiPasquale, and W. R. Boynton. 1997. Organic carbon balance and net ecosystem metabolism in Chesapeake Bay. Mar. Ecol. Prog. Ser. **150**: 229–248.

Kimmel, D. G., D. W. Miller, and M. R. Roman. 2008. Regional scale climate forcing of Mesozooplankton dynamics in Chesapeake Bay. Estuaries Coast **2**: 375–387.

Lauvset, S., N. Gruber, P. Landschützer, A. Olsen, and J. Tjiputra. 2015. Trends and drivers in global surface ocean pH over the past 3 decades. Biogeosciences **12**: 1285–1298.

Lehmann, J., D. Coumou, and K. Frieler. 2015. Increased record-breaking precipitation events under global warming. Clim. Change **132**: 501–515.

Letourneau, M. L., and P. M. Medeiros. 2019. Dissolved organic matter composition in a marsh-dominated estuary: Response to seasonal forcing and to the passage of a hurricane. Eur. J. Vasc. Endovasc. Surg. **124**: 1545–1559.

Lewis, E. R., and D. W. R. Wallace. 1998. CO2SYS-program developed for CO2 system calculations. Carbon Dioxide Information Analysis Centre. U.S. Department of Energy, Oak Ridge. doi:10.2172/639712

Li, M., L. Zhong, and W. C. Boicourt. 2005. Simulations of Chesapeake Bay estuary: Sensitivity to turbulence mixing parameterizations and comparison with observations. J. Geophys. Res. Oceans **110**: C12004. doi:10.1029/2044JC002585

Li, M., L. Zhong, W. C. Boicourt, S. Zhang, and D. Zhang. 2007. Hurricane-induced destratification and destratification in a partially-mixed estuary. J. Mar. Res. **65**: 169–192.

Li, M., and L. Zhong. 2009. Flood-ebb and spring-neap variations of mixing, stratification and circulation in Chesapeake Bay. Cont. Shelf Res. **29**: 4–14.

Li, Y., and M. Li. 2011. Effects of winds on stratification and circulation in a partially mixed estuary. J. Geophys. Res. Oceans **6**: C1202. doi:10.1029/2010JC006893

Luettich, R. A., Jr., S. D. Carr, J. V. Reynolds-Fleming, C. W. Fulcher, and J. E. McNinch. 2002. Semi-diurnal seiching in a shallow, microtidal lagoonal estuary. Cont. Shelf Res. **22**: 1669–1681.

McClain, M. E., E. W. Boyer, C. L. Dent, S. E. Gergel, N. B. Grimm, P. M. Groffman, and W. H. McDowell. 2003. Biogeochemical hot spots and hot moments at the interface of terrestrial and aquatic ecosystems. Ecosystems **6**: 301–312.

Miller, W. D., L. W. Harding Jr., and J. E. Adolf. 2006. Hurricane Isabel generated an unusual fall bloom in Chesapeake Bay. Geophys. Res. Lett. **33**: L06612. doi:10.1029/2005GL025658

Nixon, S. W. 1995. Coastal marine eutrophication: A definition, social causes, and future concerns. Ophelia **41**: 199–219.

Nixon, S. W., A. J. Oczkowski, M. E. Q. Pilson, L. Fields, C. A. Oviatt, and C. W. Hunt. 2015. On the response of pH to inorganic nutrient enrichment in well-mixed coastal marine waters. Estuaries Coast **38**: 232–241.

Osburn, C. L., L. T. Handsell, B. L. Peierls, and H. W. Paerl. 2016. Predicting sources of dissolved organic nitrogen to an estuary from an agro-urban coastal watershed. Environ. Sci. Technol. **50**: 8473–8484.

Osburn, C. L., J. C. Rudolph, H. W. Paerl, A. G. Hounshell, and B. R. Van Dam. 2019. Lingering carbon cycle effects of hurricane Matthew in North Carolina's coastal waters. J. Geophys. Res. **46**: 2654–2661. doi:10.1029/2019GL082014

Paerl, H. W., N. S. Hall, B. L. Peierls, K. L. Rossignol, and A. R. Joyner. 2013. Hydrologic variability and its control of phytoplankton community structure and function in two shallow, coastal, lagoonal ecosystems: The Neuse and New River estuaries, North Carolina, USA. Estuaries Coast **37**: 31–45. doi:10.1007/s12237-013-9686-0

Paerl, H. W., N. S. Hall, B. L. Peierls, and K. L. Rossignol. 2014. Evolving paradigms and challenges in estuarine and coastal eutrophication dynamics in a culturally and climatically stressed world. Estuaries Coast **37**: 243–258.

Paerl, H. W., J. R. Crosswell, B. Van Dam, N. S. Hall, K. L. Rossignol, C. L. Osburn, A. G. Hounshell, R. S. Sloup, and L. W. Harding Jr. 2018. Two decades of tropical cyclone impacts on North Carolina's estuarine carbon, nutrient and phytoplankton dynamics: Implications for biogeochemical cycling and water quality in a stormier world. Biogeochemistry **141**: 307–332. doi:10.1007/s10533-018-0438-x

Paerl, H. W., N. S. Hall, A. G. Hounshell, R. A. Luettich Jr., K. L. Rossignol, C. L. Osburn, and J. Bales. 2019. Recent increase in catastrophic tropical cyclone flooding in coastal North Carolina, USA: Long-term observations suggest a regime shift. Nature Sci. Rep. **9**: 10620. doi:10.1038/s41598-019-46928-9

Peierls, B. L., R. R. Christian, and H. W. Paerl. 2003. Water quality and phytoplankton as indicators of hurricane impacts on a large estuarine ecosystem. Estuaries **26**: 1329–1343.

Peierls, B. L., and H. W. Paerl. 2010. Temperature, organic matter, and the control of bacterioplankton in the Neuse River and Pamlico sound estuarine system. Aquat. Microb. Ecol. **60**: 139–149.

Peierls, B. L., N. S. Hall, and H. W. Paerl. 2012. Non-monotonic responses of phytoplankton biomass accumulation to hydrologic variability: A comparison of two coastal plain North Carolina estuaries. Estuaries Coast **35**: 1376–1392.

Piehler, M. F., L. J. Twomey, N. S. Hall, and H. W. Paerl. 2004. Impacts of inorganic nutrient enrichment on phytoplankton community structure and function in Pamlico sound, NC, USA. Estuar. Coast. Shelf Sci. **61**: 197–209.

Pinckney, J. L., H. W. Paerl, M. B. Harrington, and K. E. Howe. 1998. Annual cycles of phytoplankton community-structure and bloom dynamics in the Neuse River estuary, North Carolina. Mar. Bio. **131**: 371–381.

Qin, Q., and J. Shen. 2021. Typical relationships between phytoplankton biomass and transport time in river-dominated coastal aquatic systems. Limnol. Oceanogr. **66**: 3209–3320. doi:10.1002/lno.11874

Rothenberger, M. B., J. M. Burkholder, and C. Brownie. 2009. Long-term effects of changing land use practices on surface water quality in a coastal river and lagoonal estuary. Environ. Manag. **44**: 505–523.

Rudek, J., H. W. Paerl, M. A. Mallin, and P. W. Bates. 1991. Seasonal and hydrological control of phytoplankton nutrient limitation in the lower Neuse River estuary, North Carolina. Mar. Ecol. Prog. Ser. **75**: 133–142.

Rudolf, J. C., C. A. Arendt, A. G. Hounshell, H. W. Paerl, and C. L. Osburn. 2020. Use of geospatial, hydrologic, and geochemical modeling to determine the influence of wetland-derived organic matter in coastal waters in response to extreme weather. Front. Mar. Sci. **7**: 1–18. doi:10.3389/fmars.2020.00018

Seneviratne, S. I., and others. 2012. Changes in climate extremes and their impacts on the natural physical environment, p. 109–230. *In* C. B. Field and others [eds.], Managing the risks of extreme events and disasters to advance climate change adaptation. A Special Report of Working Groups I and II of the Intergovernmental Panel on Climate Change (IPCC). Cambridge University Press.

Shen, C., J. M. Testa, M. Li, and W. Cai. 2020. Understanding anthropogenic impacts on pH and aragonite saturation state in Chesapeake Bay: Insights from a 30-year model study. Eur. J. Vasc. Endovasc. Surg. **125**: e2019JG005620. doi:10.1029/2019JG005620

St. Laurent, K. A., V. J. Coles, and R. R. Hood. 2022. Climate extremes and variability surrounding Chesapeake Bay: Past, present, and future. J. Am. Water Resour. Assoc. **58**: 826–854. doi:10.1111/1752-1688.12945

Strickling, H. L., and D. R. Obenour. 2018. Leveraging spatial and temporal variability to probabilistically characterize nutrient sources and export rates in a developing watershed. Water Resour. Res. **54**: 5143–5162. doi:10.1029/2017WR022220

Testa, J. M., and W. M. Kemp. 2008. Variability of biogeochemical processes and physical transport in a partially

stratified estuary: A box-modeling analysis. Mar. Ecol. Prog. Ser. **356**: 63–79.

Testa, J. M., R. R. Murphy, D. C. Brady, and W. M. Kemp. 2018. Nutrient- and climate-induced shifts in the phenology of linked biogeochemical cycles in a temperate estuary. Front. Mar. Sci. **5**: 114. doi:10.3389/fmars.2018.00114

Testa, J. M., V. Lyubchich, and Q. Zhang. 2019. Patterns and trends in Secchi disk depth over three decades in the Chesapeake Bay estuarine complex. Estuaries Coasts **42**: 927–943.

Van Dam, B. R., J. R. Crosswell, I. C. Anderson, and H. W. Paerl. 2018. Watershed-scale drivers of air-water CO2 exchanges in two lagoonal North Carolina (USA) estuaries. Eur. J. Vasc. Endovasc. Surg. **123**: 271–287. doi:10.1002/2017JG004243

Van Dam, B. R., and H. Wang. 2019. Decadal-scale acidification trends in adjacent North Carolina estuaries: Competing role of anthropogenic CO2 and riverine alkalinity loads. Front. Mar. Sci. **6**: 136. doi:10.3389/fmars.2019.00136

Waldbusser, G. G., E. P. Voigt, H. Bergschneider, M. A. Green, and R. I. E. Newell. 2011. Biocalcification in the eastern oyster (*Crassostrea virginica*) in relation to long-term trends in Chesapeake Bay pH. Estuaries Coast **34**: 221–231.

Wetz, M. S., and D. W. Yoskowitz. 2013. An "extreme" future for estuaries? Effects of extreme climatic events on estuarine water quality and ecology. Mar. Pollut. Bull. **69**: 7–18. doi:10.1016/j.marpolbul.2013.01.020

Wood, S. A. 2006. Generalized additive models: An introduction with R. CRC press.

Xu, Y., W. J. Cai, R. Wanninkof, J. Salisbury, J. Reimer, and B. Chen. 2020. Long-term changes of carbonate chemistry variables along the north American East Coast. J Geophys. Res: Ocean **125**: e2019JC015982. doi:10.1029/2019JC015982

Zhang, Q., and others. 2021. Nutrient limitation of phytoplankton in Chesapeake Bay: Development of an empirical approach for water-quality management. Water Res. **188**: 116407.

Acknowledgments

Conflict of Interest

The authors declared that they have no conflict of interest to report.